Measurements of Visual Range and Radiation-Fog (Haze) Microphysics

MICHAEL B. MEYER, JAMES E. JIUSTO AND G. GARLAND LALA

Atmospheric Sciences Research Center, State University of New York, Albany NY 12222

(Manuscript received 26 June 1979, in final form 25 October 1979)

ABSTRACT

An extensive boundary-layer field program was conducted which included simultaneous measurements of visibility and particle size distributions during fog and haze. Several empirical expressions relating changes in visibility to characteristics of the aerosol (droplet) size spectrum and relative humidity are presented and evaluated. Detailed analysis of one evolving dense fog revealed several points of interest regarding the behavior of drop size spectra, including a scheme for approximating fog supersaturation.

1. Introduction

The degradation of visibility due to haze and fog has become a matter of growing concern to many groups. The transition from quasi-dry or submicron aqueous particulates (haze) to liquid droplets (fog) is directly manifested in associated changes in the visual range. Periods of radiational cooling provide ideal experimental conditions during which to measure this microphysical process since the aerosol size distribution is primarily and gradually modified by relative humidity changes. Relationships between particle size (and composition), relative humidity and visual range have, in preceding years, received a fair degree of experimental and theoretical consideration (Dessens, 1949; Junge, 1963; Garland, 1969; Hänel, 1971; Covert *et al.*, 1972). However, more needed experimental information on these interrelationships is now possible due to equipment advances and through field research conducted during radiative cooling events.

During the fall of 1977, a program was conducted on the main campus of the State University of New York at Albany to investigate visibility and droplet size spectra during periods of radiation haze and fog. Also studied, but not reported here, were numerous variables describing boundary-layer characteristics and the performance of numerical fog models. The principal objectives of the research described herein were to 1) measure representative particle (droplet) size distributions in radiation hazes and fogs of the northeastern United States (Albany, New York); and 2) relate changes in visibility to characteristics of the aerosol size spectrum and relative humidity.

2. Measurement program

a. Instrumentation and field site

Measurements of aerosol spectra generally spanned a size range from 0.3 to 15.0 μm (diameter) using two Royco optical particle counters (OPC's)—Model 225. The performance of such particle counters employing light-scattering techniques is described in the literature (e.g., Zinky, 1962; Hodkinson and Greenfield, 1965; Liu *et al.*, 1974). The Royco units were operated at a sample flow rate of 250 cm^3 min^{-1}, which for the tube orifice diameter and light to calm winds involved should permit efficient sampling of particles up to ~15–20 μm diameter (Davies, 1968). A maximum particle concentration capability of ~3000 cm^{-3} is claimed by the manufacturer; effects of index of refraction variations on particle light scattering are considered minimal in these cases of aqueous haze and fog droplets. The two instruments provided nine channels of particle size information with one common size (0.5 μm) for checking instrument consistency. In some cases, a pulse height analyzer was used in conjunction with one OPC allowing for somewhat more detailed size spectra.

A gelatin-slide impactor system (Jiusto, 1967a) was used to supplement the drop-size distribution in fog, and particularly to sample drops larger than 15 μm. Drop replicas were sized (2–46 μm) following established sampling and microscopic methods (May, 1959; Jiusto, 1967a). The standard visual range was continuously monitored at the 1.5 m level (the same height as the aerosol sampling) with an AEG-Telefunken scattered light recorder capable of

0022-4928/80/030622-08$06.00

measurements over a 0.016–65.0 km range. With this instrument light from a xenon flash lamp is scattered by particles over angles of 10° to 120° into a photomultiplier tube and the ambient extinction coefficient (and corresponding visual range via the Koschmieder equation) measured (Charlson *et. al.*, 1967).

The field site, a large grassy area, was sufficiently removed from campus buildings and roads to minimize the influences of local heat or particle sources. Housed in a 3 m × 2 m × 1.8 m metal shed were the two OPC power modules, other meteorological sensor controls, and all necessary strip chart recorders. The OPC sensor units (1.5 m level) and scattered light recorder were located a few meters from the structure. Though not used directly in this analysis, additional submicron particle size information was obtained bihourly with an electrical aerosol analyzer, a cloud condensation nucleus counter and an Aitken particle detector.

b. Data base

Fogs at Albany are principally of the radiation type (in the vicinity of high pressure systems) with a peak frequency during the months of September through early November. During the fall season local climatological data show that an average of approximately ten fogs occur with visibilities < 0.40 km (0.25 mi). The 1977 fog season produced 13 case studies at the SUNYA field site from which nine quite complete data sets were obtained. In general, aerosol particle size distributions were acquired hourly with the OPC's. During active events (i.e., large visibility changes or fog formation), sampling was increased to 30 min periods or less. Thus, these major cases include well over 100 individual aerosol measurements from which the results of this study are based.

TABLE 1. Major case studies of 1977 fog season.

Case no.	Date	Time (local)	Classification
1	10/21–10/22	2300–0730	Light fog
2	10/24–10/25	1800–0500	Light haze
3	10/27–10/28	1700–0700	Dense haze
4	10/31–11/01	1600–0700	Light haze
5	10/10–10/11	2200–1000	Dense fog
6	10/27	0800–0838	Dense fog
7	10/20–10/21	1800–0700	Light haze
8	11/09–11/10	1600–0700	Dense haze
9	10/28–10/29	1900–0800	Light haze

Each case study has been classified based on the principal variable of interest, the measured value of visual range (V). Because no standard or well-accepted visibility versus fog (haze) classification exists, the following was devised based on consideration of observing practices of the National Weather Service, the Air Weather Service, and the international definition of fog ($V < 1$ km):

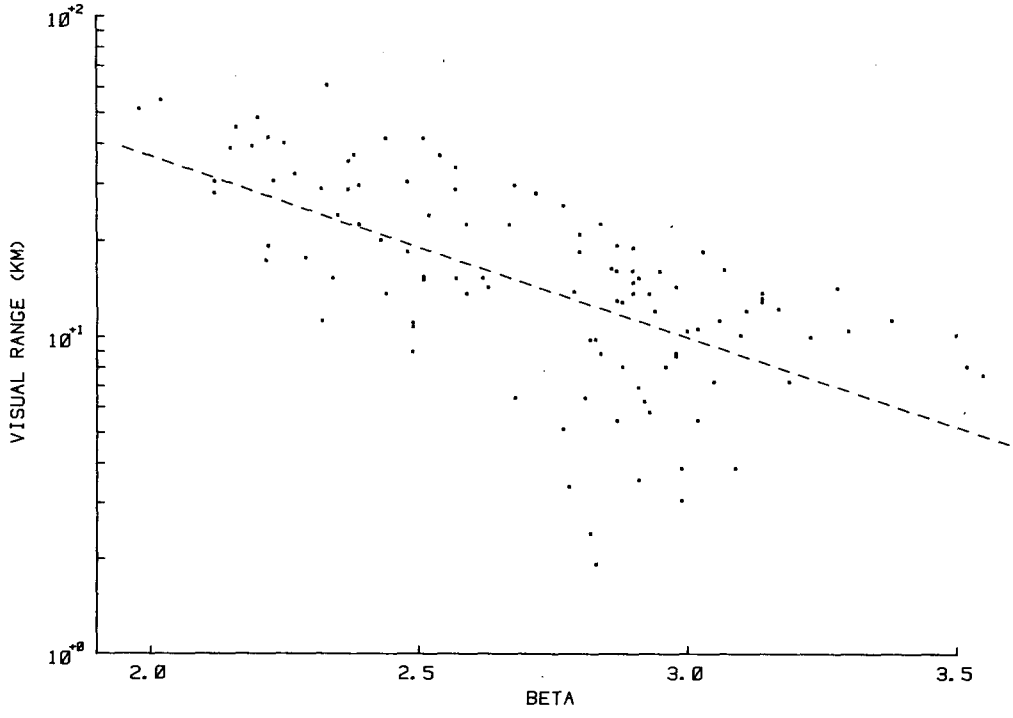

FIG. 1. Visual range versus aerosol size-distribution slope (β).

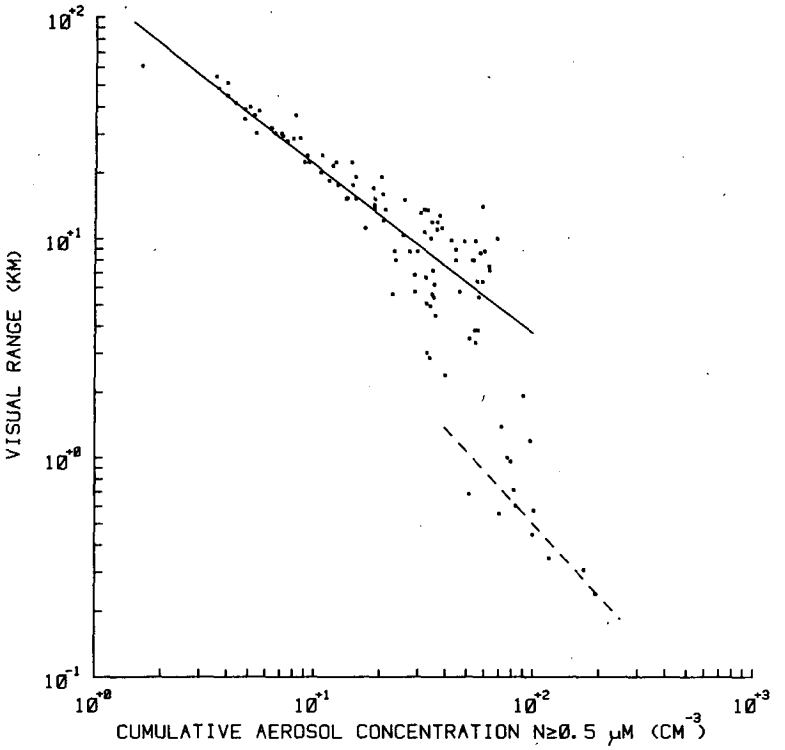

FIG. 2. Visual range versus cumulative aerosol concentration.

Classification	Visibility range (km)
Clear	$V > 16$
Light haze	$16 \geq V > 10$
Dense haze	$10 \geq V > 5$
Light fog	$5 \geq V > 1$
Dense fog	$V \leq 1$

Table 1 lists the nine major case studies by date, time and obscuration classification.

3. Results

a. *Visual range as a function of aerosol spectra characteristics*

Fig. 1 depicts visual range as a function of the slope (β) of the numerous size distributions obtained over the diameter range 0.3–15.0 μm (β being obtained from computerized graphs of cumulative number concentration versus size and the customary Junge power function $N \propto D^{-\beta}$). Unlike typical dry aerosol size distributions commonly cited in the literature, note that these distributions pertain to actual elements present—from submicron dry particles to liquid haze droplets over a broad ambient humidity range. A least-squares curve-fitting procedure yields the log-linear empirical expression for visual range V (km), i.e.,

$$V = \exp(6.2 - 1.3\beta), \quad 2 \leq \beta \leq 3.6. \qquad (1)$$

The plot does *not* include any dense fog data where the slope of the aerosol size distribution is difficult to represent by a straight line fit due to complex droplet growth characteristics. All empirical visibility functions expressed in this section implicitly include the effects of relative humidity. This is the desired situation and was made possible because the Royco sampler, as employed, is sensing *in situ* the ambient aerosol and droplets.

Eq. (1) is remarkably similar to that obtained by Glassbrook (1974) with similar apparatus at Whiteface Mountain, 130 mi north of Albany, i.e., $V = \exp(6.8-1.3\beta)$. The larger constant (6.8 vs 6.2) indicates that the visibility was lower for a given slope parameter at the Albany field site. This was probably the effect of greater concentrations of the largest Aitken nuclei (below the range of the measured spectra) present at the semi-urban Albany location.

A large spread of data points about the straight line in Fig. 1 indicates that the prediction of visual range from the slope of the aerosol distribution alone would, at best, be a crude estimate. The justification for such an empirical function, however, has some merit (Junge, 1963; Glassbrook, 1974), but obviously cannot adequately reflect more complex particle size distributions now known to occur. It does show a general decrease in visual range with increasing slope parameter β. Steeper slopes are associated with a greater increase in the concen-

tration of the smaller particles in the measurement range.

The aerosol distribution can also be described by the total concentration of particles (in this case, $N_c \geq 0.5$ μm) and some mean size. The root-mean-square (rms) diameter was employed for the mean size in accordance with Koschmeider's well-known visibility equation where droplet size squared is inversely related to visual range (Koschmeider, 1924).

Figs. 2 and 3 show the visual range plotted against cumulative aerosol concentration and rms diameter squared, respectively, for all cases except 7 and 9. The seven cases plotted include a representative cross section of visibility categories (two dense fogs, one light fog, two dense hazes, two light hazes). An inverse power relationship is evident in Fig. 2, with visual range decreasing as particle concentrations increase. However, a marked discontinuity occurs in the 1–2 km region where a second inverse power trend is indicated. This is interpreted as the transition zone from light to dense fog where drops beyond 1 μm diameter have become activated and are growing in an unstable manner. Stable haze droplets are typically less than 1 μm diameter. This transition zone at $V = 1$–2 km also coincides closely with that where the extinction of light by growing droplets reportedly loses its spectral wavelength dependence (Middleton, 1952).

Two least-squares power curve fits were computed to define simple empirical visibility-particle concentration functions for the data (Fig. 2). For haze and light fog ($V > 1$–2 km):

$$V = 120\ N_c^{-0.77}, \tag{2}$$

while for dense fog ($V \leq 1$ km):

$$V = 80\ N_c^{-1.1}, \tag{3}$$

where V is in kilometers and N_c in particles per cubic centimeter.

It is apparent that a discontinuity again exists in the 1–2 km region in Fig. 3. Mean particle size remains essentially constant at the higher visibilities (as indicated by the dashed vertical line), while below the transition zone we have the function.

$$V = 1.46 \times 10^{-4}(\bar{D}^2)^{-0.49}, \tag{4}$$

where $\bar{D}$ is the rms diameter (μm).

The previous pair of graphs (Figs. 2 and 3) clearly demonstrate that under haze conditions visibility degradation was strongly dependent on total particle concentration and influenced minimally by modest size changes in the aerosol spectra. Beyond the transition zone, however, the mean-size characteristic of the droplet aerosol was shown to be of equal, if not greater, significance in visual range reduction. Thus the physical insights provided by these empirical functions are most revealing. The absolute values of

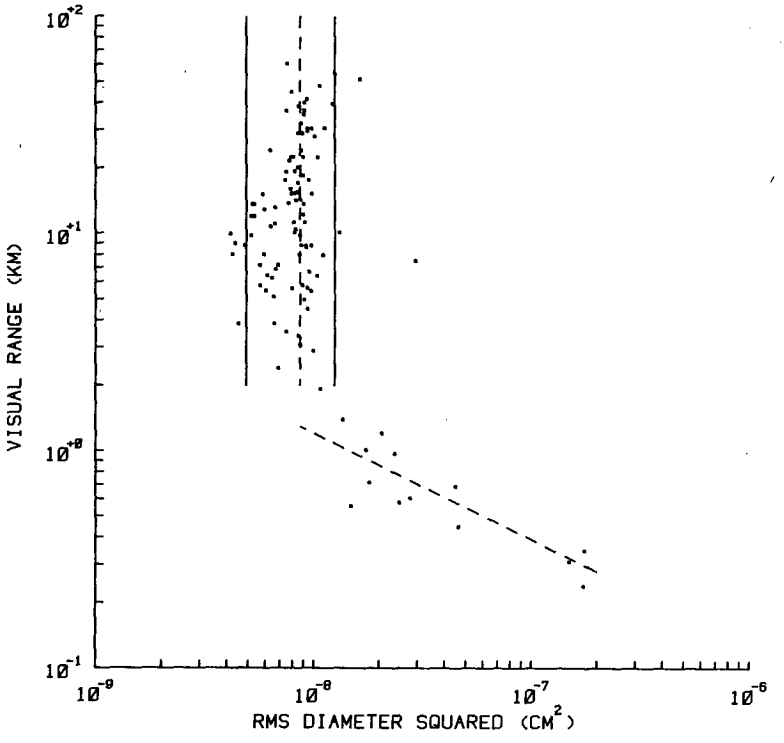

FIG. 3. Visual range versus rms diameter squared (mean surface diameter squared). Solid vertical lines indicate one standard deviation.

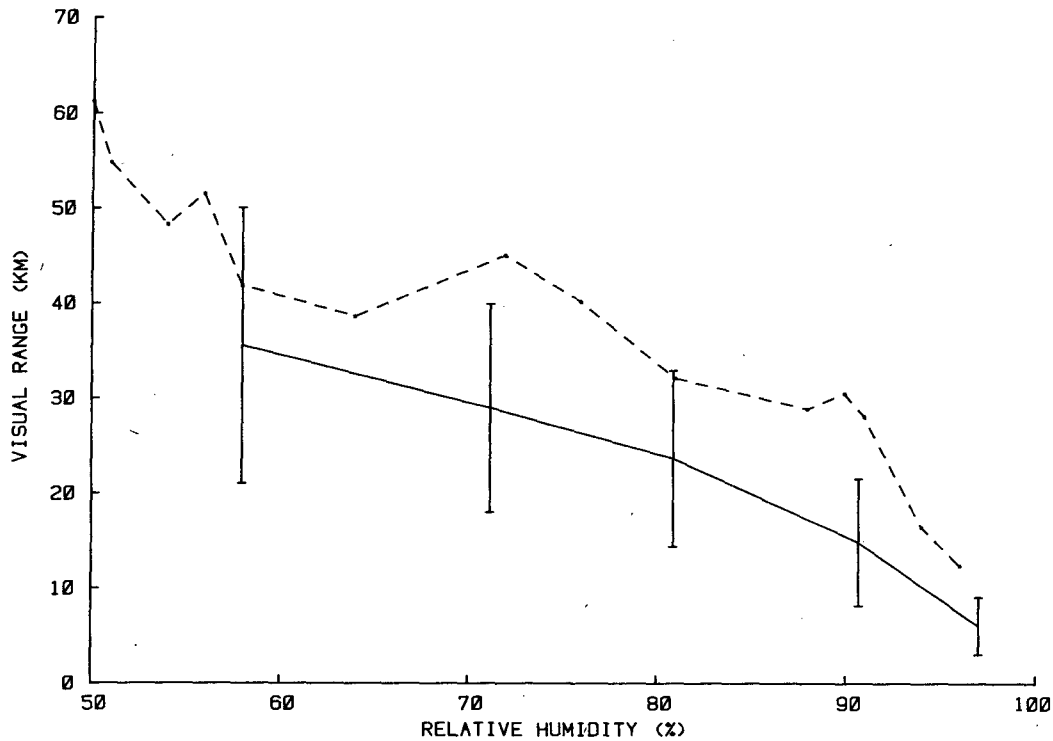

FIG. 4. Average visibility versus mean relative humidity in each relative humidity classification. (Solid vertical bars indicate one standard deviation.) Visual range versus relative humidity (case 4, dashed).

the terms undoubtedly will vary with location and with distinctly different air masses, a matter of continuing investigation.

If a constant scattering-area coefficient is assumed over the entire spectrum, then the product $N_c\bar{D}^2$ is proportional to the total scattering coefficient b (virtually equivalent to the extinction coefficient in this case). As mentioned, Koschmieder's visibility formula dictates an inverse relationship between extinction coefficient and visual range. For the data points from Figs. 2 and 3, this was, indeed, the case with the following empirical expression resulting:

$$V = 1.75 \times 10^{-5}(N_c\bar{D}^2)^{-0.86}. \quad (5)$$

The slope parameter of Eq. (5) approaches that which would be expected (-1.0), but a small change in the exponent produces a large change in V. The slope difference is perhaps due in part to the assumption of a constant scattering-area coefficient (2) which is only valid for sufficiently large particles (Johnson, 1954).

b. *Visual range as a function of relative humidity*

Fig. 4 illustrates the general trend of decreasing visual range with increasing relative humidity. The solid curve represents average visual range versus the mean relative humidity of five intervals (<65%, 66–75%, 76–85%, 86–95%, >95%). Following Hänel (1976), an empirical power law expression was computed such that

$$V = 67.7(1 - \mathrm{RH})^{0.67}, \quad (6)$$

where RH is the relative humidity in decimal form (i.e., 90% = 0.90 and $0.58 < \mathrm{RH} < 0.97$). The correlation coefficient for the fit is 0.99. The exponent (0.67) for these data compares quite favorably with that which Hänel quotes (0.64) for a continental-type aerosol. The dashed curve represents one evening's continuous measurements (case 4). Again, an overall decline in the visibility is observed with increasing relative humidity. A similar pattern often cited in the literature has been noticed at Los Angeles Airport (Neiburger and Wurtele, 1949).

For all of the data it was noticed that a wide range of visibilities could be recorded at given relative humidity readings. Thus, determination of a specific visibility-relative humidity relationship applicable for all radiational cooling events might prove a fruitless endeavor. Variations in the concentration and hygroscopicity of condensation nuclei present undoubtedly account for much of the scatter.

c. *Drop spectra evolution in a dense radiation fog*

On 11 October 1977 (case 5), under strong radiational cooling, fog commenced forming at approxi-

mately 0730L (local) and lasted until 1000L. The evolution of the aerosol (droplet) size spectra was obtained with the Royco OPC's and pulse height analyzer.

Figs. 5 and 6 show the cumulative (N_c) and differential ($dN/d\ \log D$) droplet size distributions, respectively, during fog development. Curves 1 and 2 reveal a substantial growth of droplets in only 5 min (0725 to 0730L). Apparently, when supersaturation was initially attained growth of the activated fog droplets proceeded quite rapidly. The droplet distribution continued shifting toward the larger sizes as evidenced by an increase in the number concentrations, especially above 1 μm. By 0827, when the visibility reached a minimum (curve 4, Fig. 6), a distinct bimodal distribution in the drop spectrum beyond the submicron haze region can be noticed (primary mode at 10 μm; secondary peak at ~3 μm). Additional information on the larger drops (gelatin drop-replication, Fig. 7) tends to confirm the 10 μm peak and may weakly suggest another mode around 20 μm. The presence of some

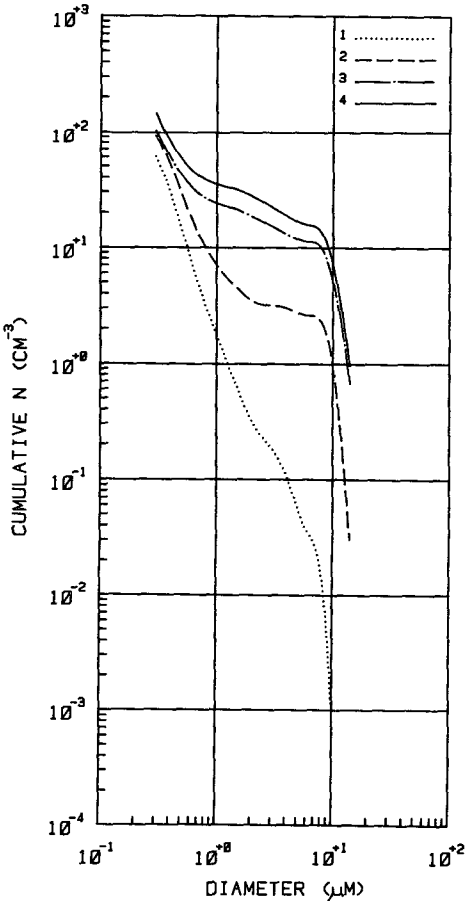

FIG. 5. Time sequence of cumulative aerosol spectra during fog development (case 5). Curve 1, 0725L, V = 2.1 km; Curve 2, 0730L, V = 1.4 km; Curve 3, 0800L, V = 0.39 km; Curve 4, 0827L, V = 0.29 km.

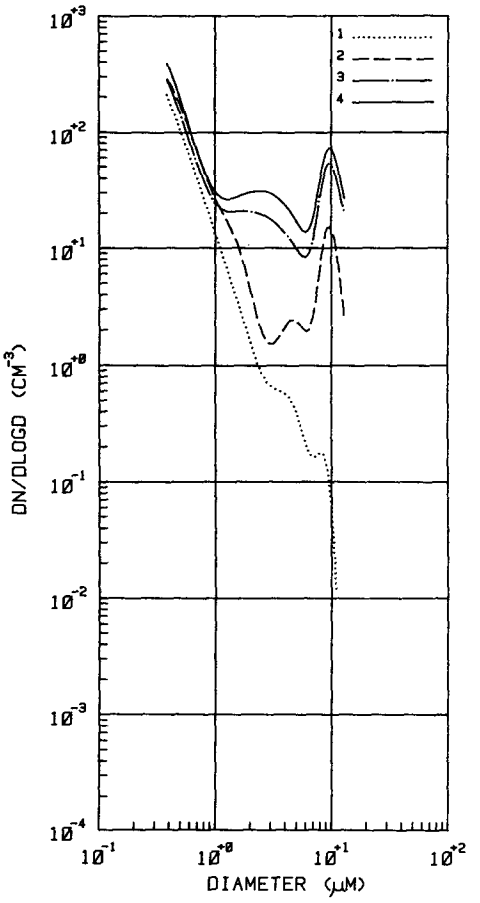

FIG. 6. Time sequence of differential aerosol spectra during fog development (case 5). Curve 1, 0725L, V = 2.1 km; Curve 2, 0730L, V = 1.4 km; Curve 3, 0800L, V = 0.39 km; Curve 4, 0827L, V = 0.29 km.

drops as large as 40 μm diameter only ~1 h after radiation fog development is indicative [from calculations employing "large" hygroscopic nuclei (Jiusto, 1967b)] of supersaturations above 0.01%.

Also evidenced in Figs. 5 and 6 is a sharp distinction between stable haze droplets and predominantly activated fog drops. Notice that the concentration of the majority of submicron haze droplets remains nearly constant over the time interval involved, while those beyond ~1.0 μm increase dramatically. This information also may be used to roughly estimate supersaturation in the fog. The drop spectrum at 0827 in Fig. 6 indicates that droplets $\geq$ 1.2 μm are actively growing. From droplet growth theory, a 1.2 μm haze droplet has an equivalent dry diameter of ~0.1 μm (assuming an ammonium sulfate nucleus). Nuclei of this size and general chemical composition require supersaturations on the order of 0.12% to become activated, thus giving an approximation of the maximum supersaturation attained in this radiation fog. At 0730 as the fog begins to form, the estimated supersaturation computed in the same

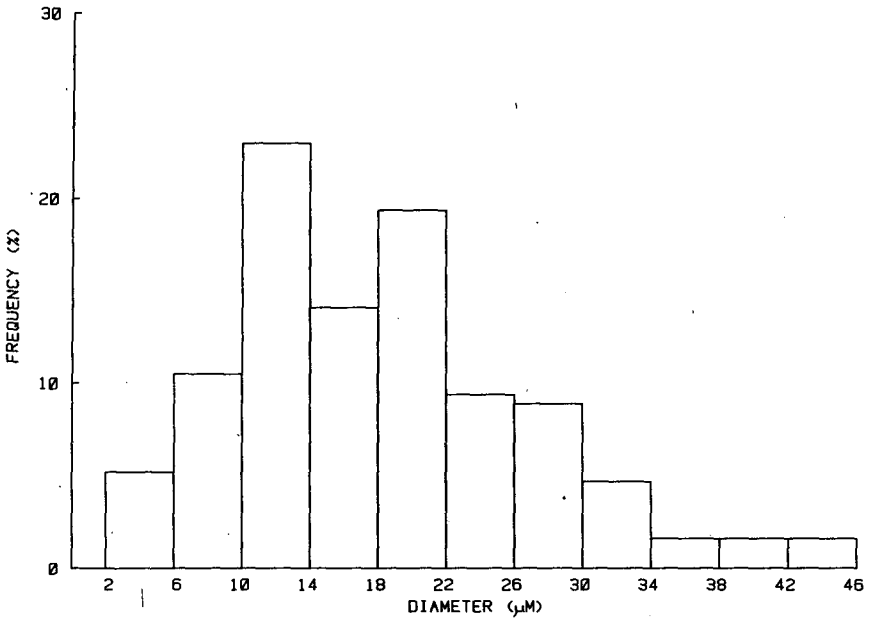

FIG. 7. Drop-size frequency distribution at 0827L (case 5).

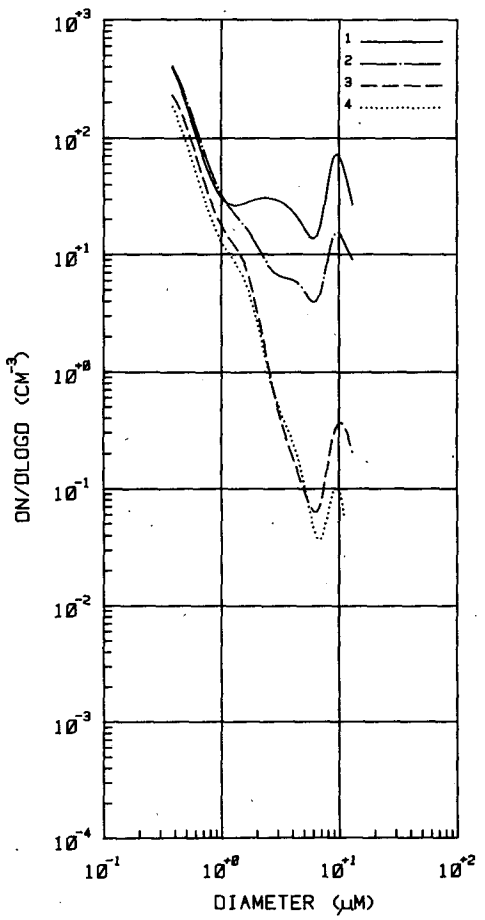

FIG. 8. Time sequence of differential aerosol spectra during fog degeneration (case 5). Curve 1, 0827L, V = 0.29 km; Curve 2, 0903L, V = 0.87 km; Curve 3, 0935L, V = 3.1 km; Curve 4, 0950L, V = 10.5 km.

way was 0.05%. Hudson (1978) has employed a different concept to estimate supersaturations of somewhat lower magnitudes (0.03–0.06) in certain coastal fogs.

The higher concentration of submicron haze particles evident in this continental fog is a feature also reported by Eldridge (1966); in marine fogs this feature sometimes can be absent (Hudson, 1978). More information is required to determine whether these several drop size modes are truly characteristic of continental radiation fogs. Rapid time variations in eddy mixing strength, low-level cooling and winds were often observed—all of which can influence resultant drop size spectra.

The differential size distribution during fog degeneration is shown in Fig. 8. (Note: curve 1 is identical to curve 4 of Fig. 6 and is included for reference purposes.) The trend observed for the development stage was essentially reversed during the fog degeneration except that the droplet peak at 10 μm persisted even after the fog intensity decreased. A similar phenomenon is present in Fig. 7 of Eldridge (1966) where haze/fog distributions were computed from spectral attenuation measurements. This peak may be slightly exaggerated due to the characteristics of this Royco counter which tends to compress the spectrum beyond 10 μm.

4. Summary

Aerosol particle size distribution measurements taken during 13 nights of radiational cooling provided an informative visibility-aerosol data set. The atmospheric particulates respond primarily to the changes in relative humidity, and this in turn directly affects atmospheric visual range.

In one dense radiation fog several points of interest were revealed:

1) Haze droplets of diameter ≥ 1.0 μm became activated to form fog droplets (corresponding maximum fog supersaturation was estimated to reach ~0.12%).

2) The number concentration of the majority of submicron haze particles (~0.3–1.0 μm) remained nearly constant throughout the life cycle of the fog.

3) There was a rapid and dramatic change in the two spectra obtained 5 min apart as visibility dropped from 2.1 to 1.4 km. This change was due to a transition from an aerosol composed primarily of haze droplets to one of haze and fog droplets.

4) At the height of fog development (minimum visibility) the drop-size spectrum exhibited a multimodal character (peaks at the submicron region and ~3, 10 and perhaps 20 μm).

5) During fog degeneration a droplet peak at 10 μm persisted even after a stable haze condition was attained.

Several empirical visual range relationships gave focus to a number of the variables that influence visibility degradation. Of particular interest is the apparent domination of aerosol concentration (as compared with size) in the determination of the visual range in haze. In fact, mean droplet size remained essentially constant until the visibility declined to 2 km or less in fog, after which drop size dominated.

Only general trends were recorded between visual range V and relative humidity and between V and the slope of the aerosol distribution; *unique* empirical relationships do not appear to be a realistic expectation.

Acknowledgment. This research was sponsored by the Atmospheric Research Section of the National Science Foundation under Grant ATM7624048.

REFERENCES

Charlson, R. J., H. Horvath and R. F. Pueschel, 1967: The direct measurement of atmospheric light scattering coefficient for studies of visibility and pollution. *Atmos. Environ.*, **1**, 469–478.

Covert, D. S., R. J. Carlson and N. C. Ahlquist, 1972: A study of the relationship of chemical composition and humidity to light scattering aerosols. *J. Appl. Meteor.*, **1**, 968–976.

Davies, C. N., 1968: The entry of aerosols into sampling tubes and heads. *J. Phys. D* (Ser. 2), **1**, 921–932.

Dessens, H., 1949: The use of spiders' threads in the study of condensation nuclei. *Quart. J. Roy. Meteor. Soc.*, **75**, 23–26.

Eldridge, R. G., 1966: Haze and fog distributions. *J. Atmos. Sci.*, **23**, 605–613.

Garland, J. A., 1969: Condensation on ammonium sulphate particles and its effect on visibility. *Atmos. Environ.*, **3**, 347–354.

Glassbrook, R. A., 1974: Standard visual range as a function of aerosol concentration and relative humidity. Atmospheric Particulates, Final Report, ASRC-SUNY Publ. No. 326, Atmospheric Sciences Research Center, State University of New York at Albany.

Hänel, G., 1971: New results concerning the dependence of visibility on relative humidity and their significance in a model for visibility forecast. *Contrib. Atmos. Phys.*, **44**, 137–167.

——, 1976: Properties of atmospheric particles as functions of relative humidity at thermodynamic equilibrium with the surrounding air. *Advances in Geophysics*, Vol. 19, Academic Press, 73–188.

Hodkinson, J. R., and J. R. Greenfield, 1965: Response calculations for light-scattering aerosol counters and photometers. *Appl. Opt.*, **4**, 1463.

Hudson, J. G., 1978: Fog microphysical measurements on the west coast. *Preprints Conf. Cloud Physics and Atmospheric Electricity*. Issaquah, Amer. Meteor. Soc., 198–205.

Jiusto, J. E., 1967a: Aerosol and cloud microphysics measurements in Hawaii. *Tellus*, **19**, 359–368.

——, 1967b: Nucleation factors in the development of clouds. Ph.D. dissertation, Pennsylvania State University, 124 pp.

Johnson, J. J., 1954: *Physical Meteorology*. The M.I.T. Press, 393 pp.

Junge, C. E., 1963: *Air Chemistry and Radioactivity*. Academic press, 382 pp.

Koschmieder, H., 1924: Theorie der horizontalen Sichtweite. *Beitr. Phys. Atmos.*, **12**, 33–53.

Liu, B. Y. H., R. N. Berglund and J. K. Agarwal, 1974: Experimental studies of optical particle counters. *Atmos. Environ.*, **8**, 717–732.

May, K. R., 1959: Detecting unvolatile airborne droplets. *Nature*, **183**, 742.

Middleton, W. E. K., 1952: *Vision through the Atmosphere*. University of Toronto Press, 250 pp.

Neiburger, M., and M. G. Wurtele, 1949: On the nature and size of particles in haze, fog, and stratus of the Los Angeles region. *Chem. Rev.*, **44**, 321–335.

Zinky, W. R., 1962: A new tool for air pollution control, the aerosol particle counter. *J. Air Pollut. Control Assoc.*, **12**, 578–583.